Monthly Notices
of the
ROYAL ASTRONOMICAL SOCIETY

MNRAS **435,** 355–367 (2013)
Advance Access publication 2013 August 7

doi:10.1093/mnras/stt1296

Magellanic Cloud stars with TiO bands in emission: binary post-RGB/AGB stars or young stellar objects?

P. R. Wood,[1⋆] D. Kamath[1⋆] and H. Van Winckel[2⋆]

[1]*Research School of Astronomy and Astrophysics, Australian National University, Cotter Road, Weston Creek, ACT 2611, Australia*
[2]*Instituut voor Sterrenkunde, K.U. Leuven, Celestijnenlaan 200D, B-3001 Leuven, Belgium*

Accepted 2013 July 15. Received 2013 July 15; in original form 2013 February 27

ABSTRACT

14 stars from a sample of Magellanic Cloud objects selected to have a mid-infrared flux excess have been found to also show TiO bands in emission. The mid-infrared dust emission and the TiO band emission indicate that these stars have large amounts of hot circumstellar dust and gas in close proximity to the central star. The luminosities of the sources are typically several thousand $L_\odot$, while the effective temperatures are ∼4000–8000 K which puts them bluewards of the giant branch. Such stars could be post-asymptotic giant branch (post-AGB) stars of mass ∼0.4–0.8 $M_\odot$ or pre-main-sequence stars (young stellar objects) with masses in the range ∼7–19 $M_\odot$. If the stars are pre-main-sequence stars, they are substantially cooler and younger than stars at the birth line where Galactic protostars are first supposed to become optically visible out of their molecular clouds. They should therefore be hidden in their present evolutionary state, although this problem may be overcome if asymmetries are invoked or if the reduced metallicity of the Small Magellanic Cloud and Large Magellanic Cloud compared to the Galaxy makes the circumstellar material more transparent. The second explanation for these stars is that they are post-AGB or post-red giant branch stars that have recently undergone a binary interaction when the red giant of the binary system filled its Roche lobe. Being oxygen-rich, they have gone through this process before becoming carbon stars. Most of the stars vary slowly on time-scales of 1000 d or more, suggesting a changing circumstellar environment. Apart from the slow variations, most stars also show variability with periods of tens to hundreds of days. One star shows a period that is rapidly decreasing and we speculate that this star may have accreted a large blob of gas and dust on to a disc whose orbital radius is shrinking rapidly. Another star has Cepheid-like pulsations of rapidly increasing amplitude, suggesting a rapid rate of evolution. Seven stars show quasi-periodic variability and one star has a light curve similar to that of an eclipsing binary.

Key words: stars: AGB and post-AGB – stars: emission-line, Be – stars: pre-main-sequence.

1 INTRODUCTION

As part of an optical spectral survey of post-asymptotic giant branch (post-AGB) candidates in the Magellanic Clouds (MCs), we have discovered 14 stars that show bandheads of the TiO molecule in emission. The post-AGB candidates were selected because they had excess mid-infrared (mid-IR) emission in their spectral energy distributions (SEDs), indicating the presence of circumstellar dust, and presumably gas.

Normal red giant or main-sequence stars with effective temperatures $T_{\rm eff} \lesssim 3800$ K (the M stars) show TiO bands in absorption. However, a small number of stars have previously been found to show TiO bands in emission. Covey et al. (2011) and Hillenbrand et al. (2012) have found three nearby young stellar objects (YSOs) which show TiO bands in emission. These stars have various other emission lines, especially Hα, and Covey et al. (2011) and Hillenbrand et al. (2012) argue that their YSOs have accretion discs and that the TiO band emission comes from dense circumstellar gas with $n \gtrsim 10^{10}$ cm^{-3} and $T \sim$ 1400–4000 K in the accretion disc. An earlier study by Zickgraf et al. (1989) found four Be stars in which they tentatively identified emission in the TiO bandhead at 6159 Å (our spectra of some of these Be stars, to be published elsewhere, show additional bandheads of TiO at longer wavelengths, confirming the findings of Zickgraf et al. 1989). The Be stars also show a mid-IR flux excess in their SEDs and are known to be surrounded by discs of dust and gas (e.g. Porter & Rivinius 2003). Zickgraf et al. (1989) estimate a gas density greater than $\sim 10^9$ cm^{-3} for the circumstellar gas in their stars with TiO bands in emission.

⋆E-mail: wood@mso.anu.edu.au (PRW); devika13@gmail.com (DK); Hans.VanWinckel@ster.kuleuven.be (HVW)

Both YSOs and Be stars which show TiO band emission have been found to also show the first overtone band of the CO molecule in emission at 2.3 μm (Zickgraf et al. 1989; Hillenbrand et al. 2012).

The common feature linking the YSOs and Be stars is a circumstellar disc and it therefore seems that a circumstellar disc of gas and dust is an essential component for the production of TiO band emission and the unusual temperature structure it requires. A common feature of binary post-AGB stars is the presence of a circumbinary disc (e.g. Van Winckel 2004; de Ruyter et al. 2006), so these stars could also potentially show TiO bands in emission. Here, we describe objects with TiO band emission in the MCs that are possible post-AGB or post-red giant branch (post-RGB) star binaries, or YSOs.

2 OBSERVATIONS AND DATA REDUCTION

Full details of the selection of objects, spectral observations, data reduction and estimation of luminosity and $T_{\rm eff}$ are given by Kamath, Wood & Van Winckel (2013). In brief, post-AGB candidates were selected using photometry of MC stars from the *Spitzer Space Telescope* surveys SAGE (Meixner et al. 2006) and SAGE-SMC (Gordon et al. 2011) combined with optical *UBVI* photometry from Zaritsky et al. (2002) for the Small Magellanic Cloud (SMC) and Zaritsky et al. (2004) for the Large Magellanic Cloud (LMC). Candidates were selected mostly for their strong 24 μm and/or 8 μm flux excesses. Optical spectra were taken with the multifibre AAOmega spectrograph (Smith et al. 2004) and have a resolution of ∼1300 and a wavelength range of ∼3700–8800 Å. A computer program was created which automatically derived $T_{\rm eff}$, $\log g$ and [Fe/H] by comparing the observed spectra to synthetic spectra from Munari et al. (2005). Given the large amount of molecular band emission superimposed on our observed spectra, additional uncertainties are associated with the parameters derived by this procedure. We therefore also made eye-estimates of the spectral type using the spectral features in the interval ∼3700–4700 Å shown in Gray & Corbally (2009) (predominantly Balmer lines, Ca II H&K lines and the *G* band). $T_{\rm eff}$ was then computed using the ($T_{\rm eff}$, spectral type) relation given by Pickles (1998).[1] Table 1 lists these values of $T_{\rm eff}$ along with spectral types and the automatically derived values of $T_{\rm eff}$, $\log g$ and [Fe/H]. In general, the two values of $T_{\rm eff}$ are reasonably similar.

The luminosities of the central stars were computed in two ways. First, after removing a foreground extinction corresponding to $E(B-V) = 0.08$ and 0.12 (Keller & Wood 2006) for the LMC and SMC, respectively, and using the extinction law of Cardelli, Clayton & Mathis (1989), the apparent luminosity was computed by integrating under the SED made from the photometry described above, along with *WISE* photometry in the *W1–W4* bands (Wright et al. 2010). The absolute luminosities $L_{\rm obs}$ were then obtained by applying distance moduli of 18.54 and 18.93 (Keller & Wood 2006) for the LMC and SMC, respectively. We also note that the heliocentric radial velocities of all the stars (Table 1) are consistent with the membership of the MCs so the adopted distance moduli are appropriate.

For circumstellar dust that is not in a spherically symmetric distribution, $L_{\rm obs}$ could be either an overestimate or an underestimate. For example, in the case of a dense disc obscuring the central star but only capturing a fraction of the 4π sr of photospheric emission,

[1] A convenient tabulation is given at http://www.stsci.edu/hst/HST_overview/documents/synphot/AppA_Catalogs5.html.

Table 1. Properties of the objects.

Name	SpT	$T_{\rm eff}$	v (km s^{-1})	$T_{\rm eff}$	$\log g$ (cgs)	[Fe/H]	$E(B-V)$	$L_{\rm obs}$ ($L_\odot$)	$L_{\rm phot}$ ($L_\odot$)	Star type	Period (d)	Hα emission	Li absorption
J004805.01−732543.0	K	4–5000	199	3849	0.0	−1.05	0.16	3492	1960	p-RGB	1150→400	Yes	?
J004843.76−735516.8	G0	5500	183	5337	0.8	−1.46	0.09	10 067	7677	?	114, 164	No	No
J005355.00−731900.9	K2	4250	189	4140	0.0	−1.38	0.30	2869	2385	p-RGB	193	Yes	Strong
J005504.57−723451.1	A2	8900	183	7480	3.0	−1.0	0.10	2148	2220	PMS	–	Resolved	No
J005514.24−732505.3	F5	6640	163	6404	2.5	−1.0	0.18	3486	743	PMS	206	Yes	No
J005529.48−715312.2	F0	7690	178	6457	2.1	−0.39	0.37	5141	6668	PMS	–	No	No
J010324.36−723803.5	G0	5500	189	4447	0.0	−1.16	0.06	28 384	21757	p-AGB	–	No	No
J010628.81−715204.8	A5	8450	191	7443	2.5	−1.0	0.24	5031	4988	PMS	33.5	P Cyg	No
J010929.79−724820.6	K5	4000	129	4173	0.7	−1.02	0.33	3079	3732	?	444[a], 100, 69.7	No	?
J050747.45−684351.2	K0	4850	267	5430	0.5	−1.36	0.34	1304	2068	p-RGB	–	P Cyg	?
J051155.66−693020.6	K0	4850	245	4096	0.0	−0.9	0.04	1865	1618	p-RGB	–	–	?
J051516.28−685539.7	K:	4–5000	311	3878	0.0	−1.06	0.19	3529	2943	p-AGB	380[a], 124	No	Strong
J052023.97−695423.2	GK::	4–6000	324	5244	2.0	−2.5	0.17	2907	626	PMS	–	Resolved	No
J052230.40−685923.9	GK::	4–6000	299	4493	1.6	−0.97	0.51	2876	3375	PMS	46	No	Strong

Notes. 'SpT' is the eye-estimated spectral type, 'v' is the heliocentric radial velocity and 'Star type' is the estimated evolutionary status based on $\log g$ (p-RGB for a binary post-RGB star; p-AGB for a binary post-AGB star; PMS for a PMS star and '?' if we could not derive the type from $\log g$). 'Star type' is quite uncertain (see text).
[a]Long secondary period.

$L_{\rm obs}$ will be an underestimate of the total emission, while if the disc is oriented so that its pole points to the observer, $L_{\rm obs}$ will be an overestimate.

The second method of computing the luminosity of the central star has several steps. First, the intrinsic colours of the central star were derived from the estimated $T_{\rm eff}$ (the automatically derived $T_{\rm eff}$ was used). The reddening was then derived by finding the value of $E(B-V)$ that minimized the sum of the squared differences between the dereddened observed and the intrinsic *B, V, I* and *J* magnitudes. The Cardelli et al. (1989) extinction law[2] was used. Using the derived $E(B-V)$, the observed magnitudes were corrected for extinction. Then the *BVIJ* fluxes of the best-fitting model atmosphere from the $T_{\rm eff}$ estimation procedure were normalized to the corrected *BVIJ* fluxes. The bolometric correction to *V* for the model atmosphere, coupled with the distance moduli to the LMC and SMC then allowed the derivation of the photospheric luminosity $L_{\rm phot}$. We note that this luminosity should be free from errors caused by asymmetry in the circumstellar dust distribution except when there is a substantial non-photospheric flux in the *BVIJ* bands from emission or scattering by circumstellar matter. This is known to occur in some cases, e.g. in the bipolar post-AGB star known as the Red Rectangle (Cohen et al. 2004). There will also be uncertainties in the luminosity arising from errors in the estimation of $T_{\rm eff}$. A comparison of $L_{\rm phot}$ and $L_{\rm obs}$ gives some estimate of the errors involved: a large difference between the two values, which occurs in two cases, suggests a non-spherical distribution of circumstellar dust. Both $L_{\rm phot}$ and $L_{\rm obs}$ are listed in Table 1 together with the total reddening $E(B-V)$ to the photosphere estimated as described above.

3 RESULTS

3.1 Spectral energy distributions

The observed broad-band magnitudes of the objects from *U* to 24 μm are given in Table 2. In Figs 1 and 2, the SEDs corresponding to the observed magnitudes are shown by red points, while the SEDs corresponding to the dereddened magnitudes are shown by blue points. Also shown in each plot is the energy distribution of the best-fitting model atmosphere. In most cases, the dereddened SED consists of the photospheric emission from the central star and moderate amounts of excess mid-IR emission at wavelengths longer than ∼1.2 μm. This is as expected for stars surrounded by dust that absorbs a fraction of the photospheric flux and re-emits it in the near- to mid-IR. The dust could be in a disc or a close-in circumstellar shell.

The SED of the star J005514.24−732505.3 is very unusual, with the mid-IR luminosity dominating the photospheric luminosity. The luminosity $L_{\rm obs}$ obtained by integrating under the SED for J005514.24−732505.3 is approximately five times the luminosity $L_{\rm phot}$ estimated for the photosphere of the optically-visible star. For a single star, this luminosity ratio requires a special geometry with a thick disc seen edge-on. The disc obscures the central star whose optical light is seen mainly by scattering of light emerging through the poles of the disc. From detailed modelling, Men'shchikov et al. (2002) state that $L_{\rm obs}$ can be several times $L_{\rm phot}$ in this case. Another possibility is that there is a second *luminous*

[2] It is possible that the circumstellar extinction law is different from the interstellar extinction law, but we have not explored this possibility. For example, Cohen et al. (2004) adopt a grey circumstellar extinction law for the Red Rectangle due to very large grains in the circumbinary disc.

Table 2. Photometry of the objects.

Name	*U*	*B*	*V*	*I*	*J*	*H*	*K*	*W1*	[3.6]	[4.5]	*W2*	[5.8]	[8.0]	*W3*	*W4*	[24]
J004805.01−732543.0	...	19.321	17.282	15.838	13.853	12.737	12.121	11.055	10.832	10.278	10.315	9.733	8.968	8.287	7.080	7.275
J004843.76−735516.8	15.714	15.091	14.434	13.290	12.733	12.023	11.572	10.733	10.670	10.289	10.219	9.948	9.442	8.790	8.117	7.942
J005355.00−731900.9	19.640	18.682	16.955	14.982	13.909	12.928	12.454	11.611	11.437	10.988	10.964	10.456	9.902	9.286	7.360	8.451
J005504.57−723451.1	15.607	15.824	15.592	15.217	14.876	14.557	14.211	13.434	13.184	12.721	12.824	12.341	11.672	11.313	9.379	...
J005514.24−732505.3	17.840	17.548	17.072	16.470	15.776	14.205	12.699	10.702	10.347	9.661	9.652	8.999	8.338	7.794	6.791	6.716
J005529.48−715312.2	16.375	16.029	15.239	14.310	13.683	13.191	12.739	11.370	11.314	10.586	10.535	9.835	8.775	7.787	5.938	5.855
J010324.36−723803.5	15.733	14.904	13.556	12.168	11.373	10.661	10.374	9.567	9.510	9.018	8.971	8.423	7.831	7.272	6.377	6.408
J010628.81−715204.8	15.719	15.411	15.135	14.570	14.092	13.680	12.997	11.455	11.178	10.469	10.429	9.767	8.853	7.878	5.694	5.626
J010929.79−724820.6	20.114	18.150	16.469	14.641	13.512	12.602	12.398	12.221	12.186	11.955	12.110	11.612	11.222	11.018	9.398	9.657
J050747.45−684351.2	17.751	17.272	16.172	15.099	14.267	13.640	13.408	12.333	12.620	12.193	12.044	11.756	11.184	11.364	9.856	9.542
J051155.66−693020.6	19.541	17.898	16.114	14.843	13.946	13.254	12.821	12.025	11.730	11.097	11.245	10.539	9.794	9.167	8.869	7.974
J051516.28−685539.7	20.124	18.046	16.190	14.369	13.236	12.306	12.011	11.099	11.013	10.358	10.339	9.687	8.838	8.066	6.813	6.854
J052023.97−695423.2	18.424	18.246	17.063	16.090	15.630	14.937	13.803	11.723	...	10.341	10.347	9.491	8.442	7.027	3.786	3.620
J052230.40−685923.9	...	18.147	16.547	14.584	13.493	12.510	12.030	...	10.927	10.492	...	10.009	9.468	...	...	7.933

Notes. U, B, V and *I* magnitudes from Zaritsky et al. (2002), *J, H, K*, [3.6], [4.5], [5.8], [8.0] and [24] from the SAGE (Meixner et al. 2006) and SAGE-SMC (Gordon et al. 2011) catalogues, and *W1, W2, W3* and *W4* from the *WISE* catalogue. Where no magnitude exists, a value of ... is given.

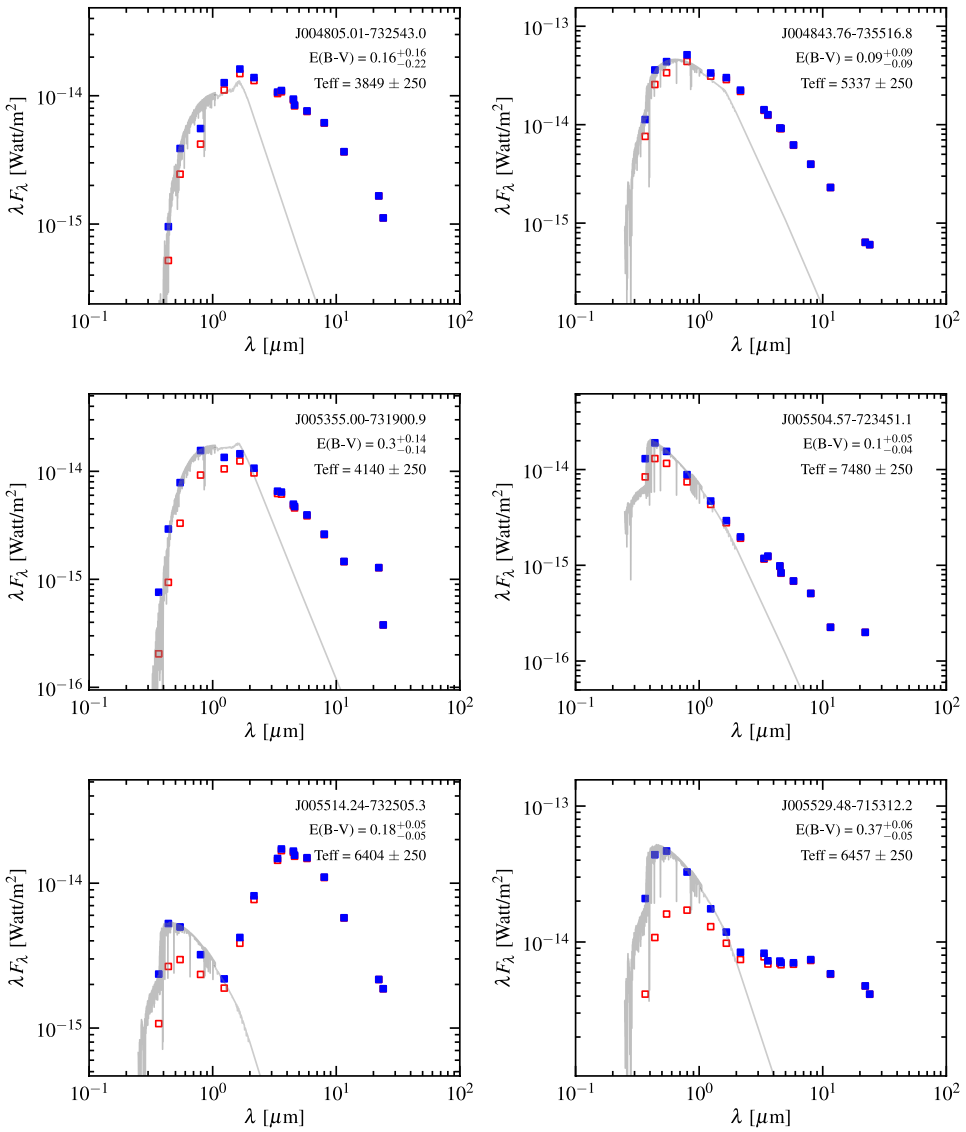

Figure 1. SEDs of the first six sources. The red open squares show the observed broad-band photometry, while the blue filled squares show the dereddened photometry. For wavelengths up to 1.05 μm, the best-fitting Munari synthetic spectrum is plotted, while for longer wavelengths the low-resolution flux distribution from the corresponding atmospheric model of Castelli & Kurucz (2004) is plotted.

star embedded with the observed star, or there is another independent object coincident on the sky with the optically observed star. The object J052023.97−695423.2 has a similarly large $L_{\rm obs}$. For it, $L_{\rm obs}$ is ∼2.8 times the luminosity $L_{\rm phot}$. J052023.97−695423.2 has previously been classified as a high-probability YSO candidate – see Section 3.3.

3.2 Optical spectra

The full observed optical spectra for the objects studied here are shown in Fig. 3. The absolute flux values for the spectra were obtained by matching the relative fluxes of the observed spectra to the photometric *B, V* and *I* values. A range of spectral types are present, from hot stars with strong Balmer absorption lines to cool stars with calcium triplet lines in absorption but no Paschen lines.

TiO band emission is prominent in all the spectra. In order to see the TiO emission better, the spectra were divided by a low-order polynomial fit to the continuum. They were then re-plotted from 6000 to 8700 Å in Fig. 4. The top panel of Fig. 4 shows the spectrum of a late M star with the position of TiO and VO absorption bands marked. It is clear that for the objects being studied here, there is TiO emission in most of the TiO bands in the spectral region shown. It is not clear that there is any VO band emission. The existence of this emission indicates the presence near the central star of molecular gas with a temperature less than ∼4000 K and with a temperature profile that increases towards the observer. The origin of this temperature structure is unclear – see Hillenbrand et al. (2012) for a discussion of possibilities.

About half the spectra also show Hα in emission (see Table 1 and Figs 3 and 4). The Hα emission in J010628.81−715204.8 and J050747.45−684351.2 shows a P Cygni profile corresponding to wind terminal velocities of approximately 430 and 350 km s^{-1}, respectively. J010628.81−715204.8 also shows the calcium triplet lines in emission. The Hα emission lines in J005504.57−723451.1 and J052023.97−695423.2 are resolved, and their observed

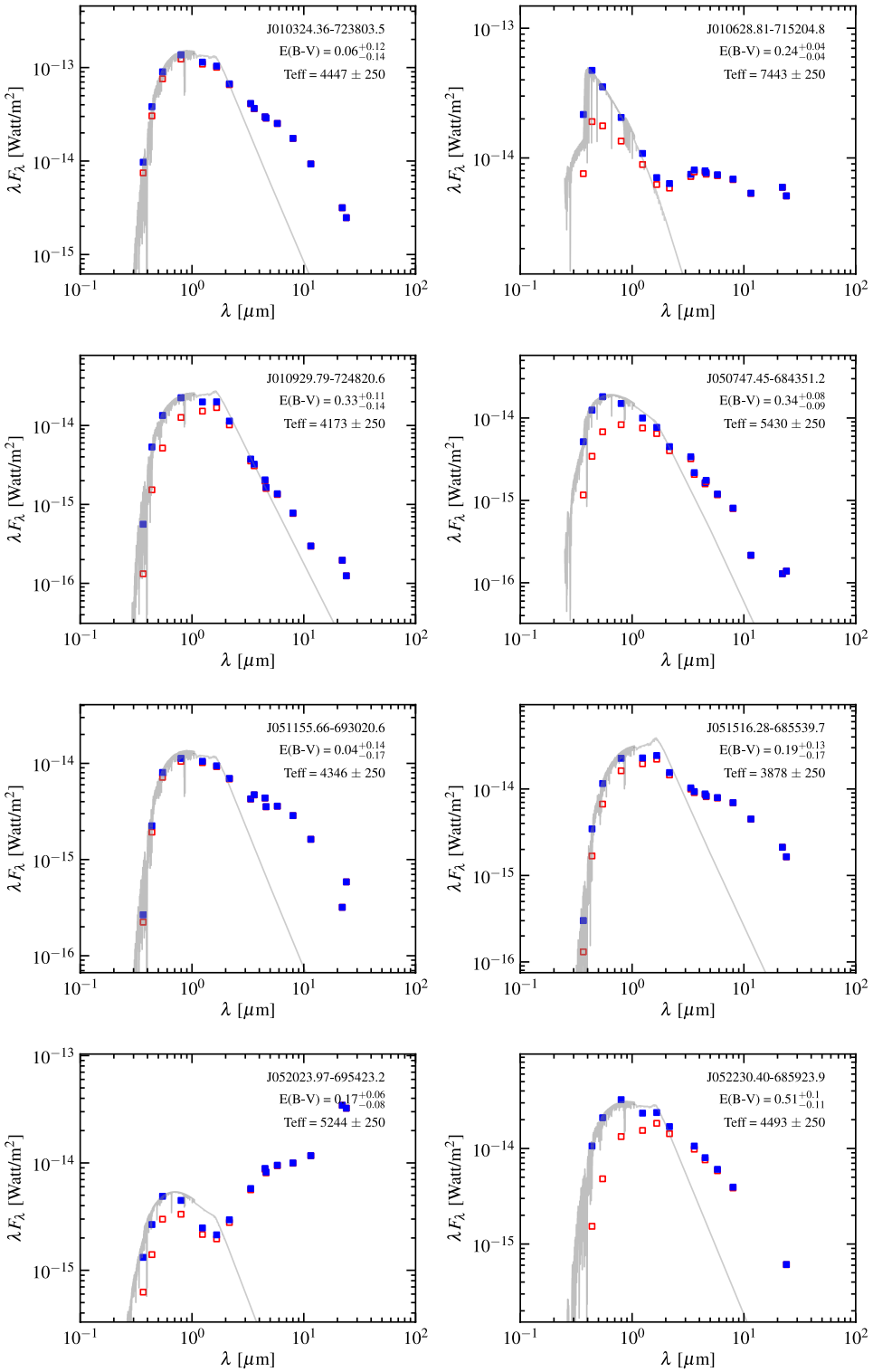

Figure 2. SEDs of the remaining eight sources.

profiles correspond to the instrumental profile convolved with Gaussian velocity distributions of standard deviation 100 and 180 km s^{-1}, respectively. The Hα emission in J052023.97−695423.2 also has broad wings extending out to 900 km s^{-1}. We note that Hα emission is common in YSOs with discs that are accreting surrounding gas (Appenzeller & Mundt 1989), but it is also common in post-AGB stars (van de Steene, Wood & van Hoof 2000).

In some stars, the [O III] 5007 Å emission line can be seen. This is most likely LMC background emission not associated with the object. Such emission is very hard to remove with a multifibre

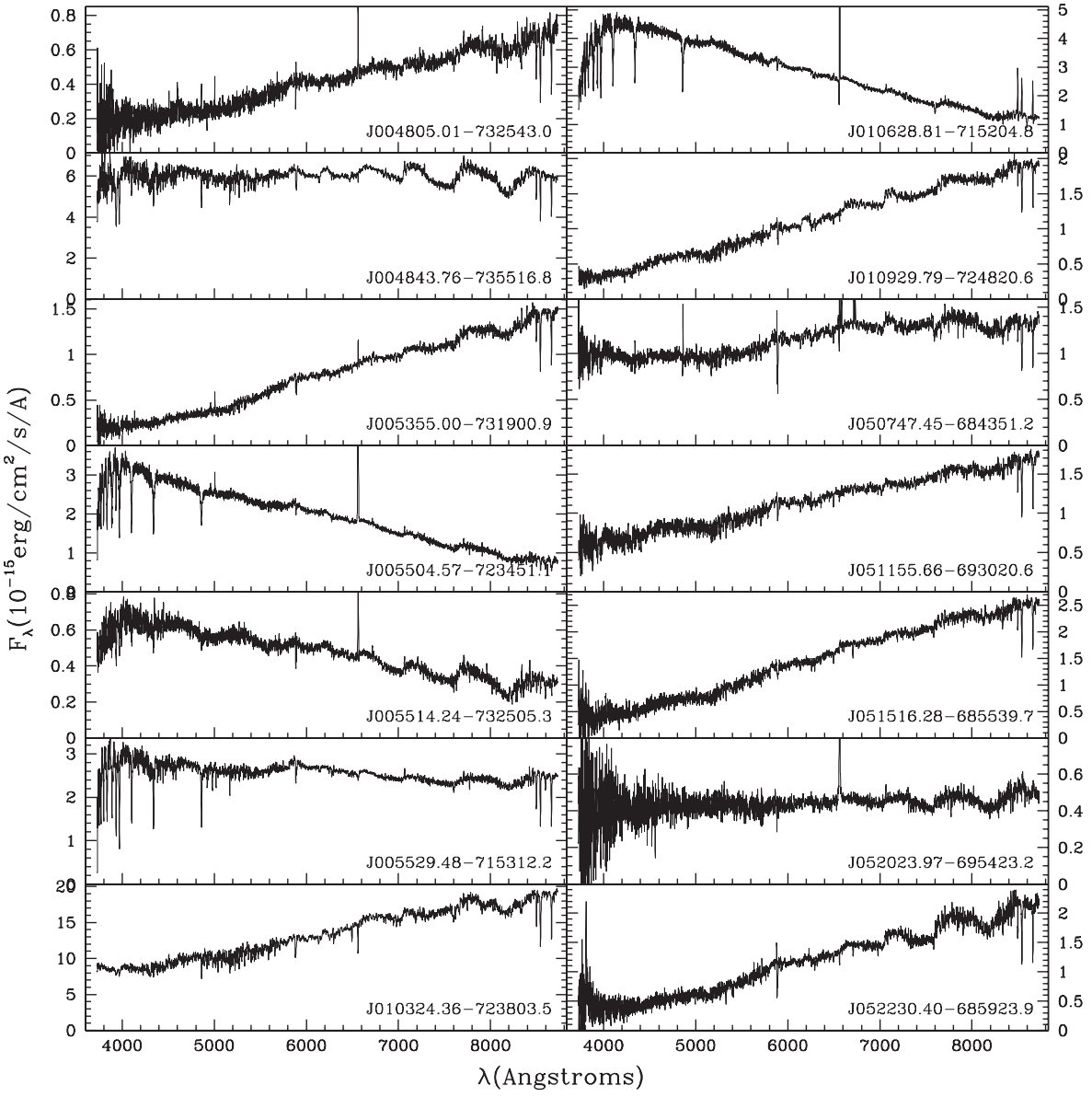

Figure 3. The spectra of the objects showing TiO bands in emission.

spectrograph which samples the sky at random points over a 2° field.

3.3 The stars in the Hertzsprung–Russell diagram

The stars are shown in the Hertzsprung–Russell (HR) diagram in Fig. 5 along with evolutionary tracks for pre-main-sequence (PMS) stars, normal post-main-sequence stars, and post-AGB and post-RGB stars. Both L_{obs} and L_{phot} values are shown. In general, these two values do not differ greatly compared to the overall spread in luminosity values, except for the two stars mentioned in Section 3.1 where the dust is most likely in a thick edge-on disc or where a second object may be contributing to L_{obs}, thereby making it too large.

For the range of observed luminosities, it is possible to explain the stars as either PMS stars, normal post-main-sequence stars on helium core burning loops, or post-AGB or post-RGB stars. However, given that our observed stars all have large amounts of hot circumstellar material, it is unlikely that they are in the rather quiet evolutionary stage of helium core burning. The most likely stars to have mass-loss and an IR excess in this evolutionary phase are Cepheid variables. Yet, observations of these stars in the LMC (Neilson et al. 2010) show the mid-IR excess flux at 8 μm in these stars is about 10 per cent of the photospheric continuum, whereas in the present group of objects the mid-IR excess flux at 8 μm is typically about 10 times the photospheric continuum. We therefore reject the explanation of these stars as normal post-main-sequence stars.

The other possible evolutionary states for these objects are post-AGB or post-RGB stars, or PMS stars.[3] In both the post-RGB and post-AGB cases, the observed stars must have undergone a binary interaction in order for them to have left their respective giant

[3] In this paper, we use the term PMS star to describe the star itself, while we use the term YSO to describe the PMS star and its surrounding dust and gas. The term post-AGB star or post-RGB star can mean either the star itself or the star and its surrounding dust and gas.

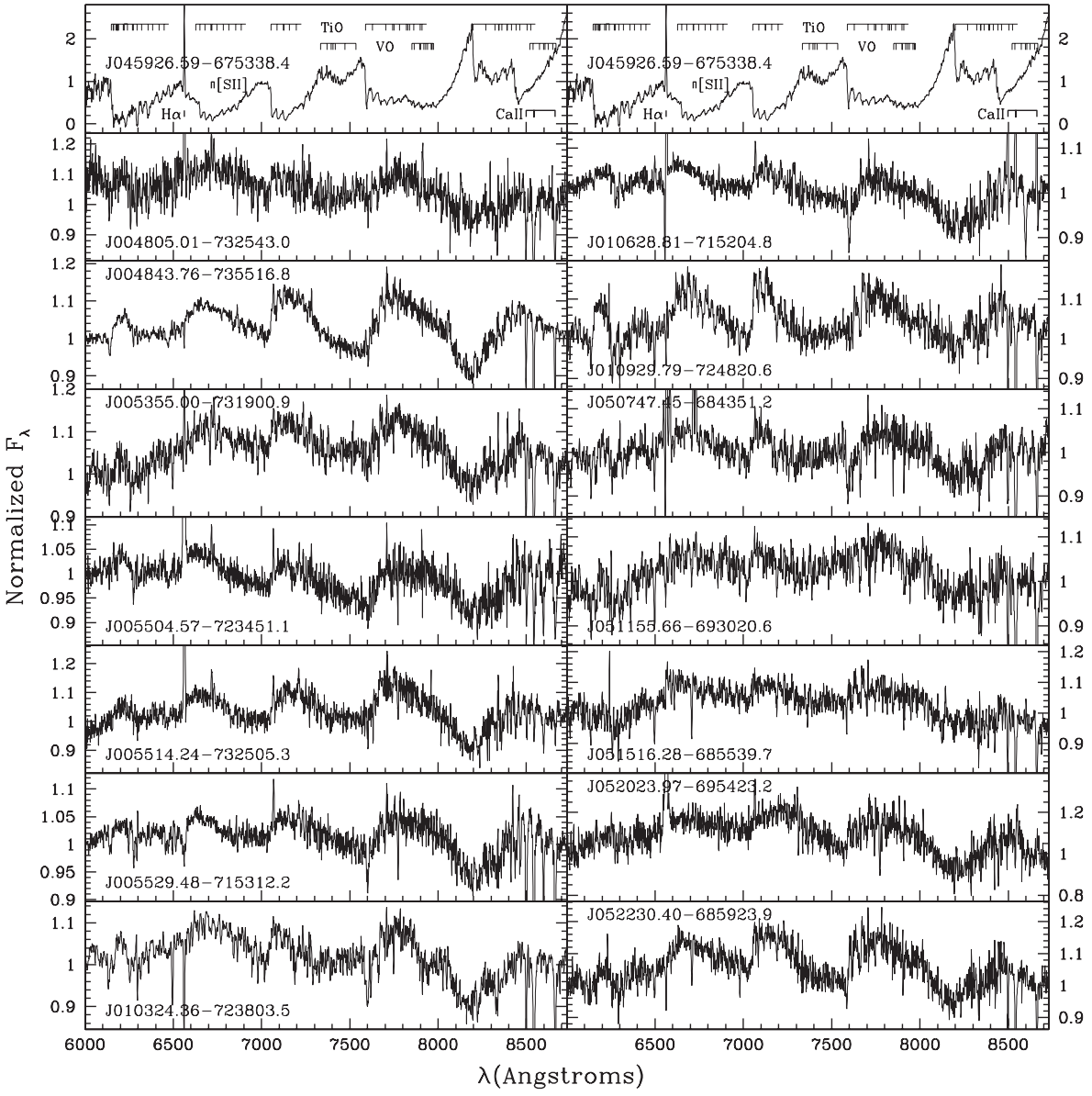

Figure 4. The continuum-normalized spectra from 6000 to 8700 Å. Also shown is the spectrum of a late M star with the positions of band heads of the TiO and VO molecules marked. The positions of Hα, the [S II] lines at 6717 and 6731 Å, and the Ca triplet lines are also shown.

branches. For RGB stars, which have luminosities $L < 2500\,L_\odot$, single-star mass-loss is insufficient to remove the H-rich envelope and produce a post-RGB star (Vassiliadis & Wood 1993). The only way large amounts of mass-loss and evolution off the RGB can occur is via binary interaction, presumably a common envelope event that leaves the binary in a tighter orbit than the original one (e.g. Han, Podsiadlowski & Eggleton 1995). For AGB stars, large amounts of mass-loss can occur either by binary interaction or, for single stars, by the very high mass-loss rate 'superwind' that terminates AGB evolution (e.g. Vassiliadis & Wood 1993). However, in the MCs, all the single stars with high mass-loss rates, at least for $\log L/L_\odot < 4.3$, are carbon stars (e.g. Blum et al. 2006; Groenewegen et al. 2007; Gordon et al. 2011). Given that the stars in the present sample are oxygen-rich because they show TiO molecules in their spectra, we believe that only binary interaction could explain a post-AGB status.

It is not easy to distinguish between post-RGB/AGB binaries and PMS stars. Both are surrounded by large amounts of circumstellar gas which is accreting (or re-accreting in the case of post-RGB/AGB stars) on to a circumstellar or circumbinary disc. However, a distinguishing feature is the gravity of the central star. We note that, at a given luminosity, the mass of a PMS star is about 15–20 times that of the corresponding post-RGB/AGB star. This leads to a difference of ∼1.3 in $\log g$ between PMS stars and post-RGB/AGB stars. The errors in our $\log g$ estimates for individual stars are typically 0.5 (Kamath et al. 2013), although the presence of strong TiO emission bands in the current set of stars almost certainly increases the error. Given the expected $\log g$ difference, we can use the derived $\log g$ values in Table 1 to make a tentative assignment of PMS or post-RGB/AGB status. This evolutionary status, PMS or post-RGB/AGB, is given in Table 1. The distinction between the post-RGB and post-AGB status is based on whether $L_{\rm phot}$ is less than or greater than, respectively, the RGB tip luminosity $L \approx 2500\,L_\odot$. We estimate that there are four post-RGB stars, two post-AGB stars and six PMS stars, the latter including the four stars hotter than

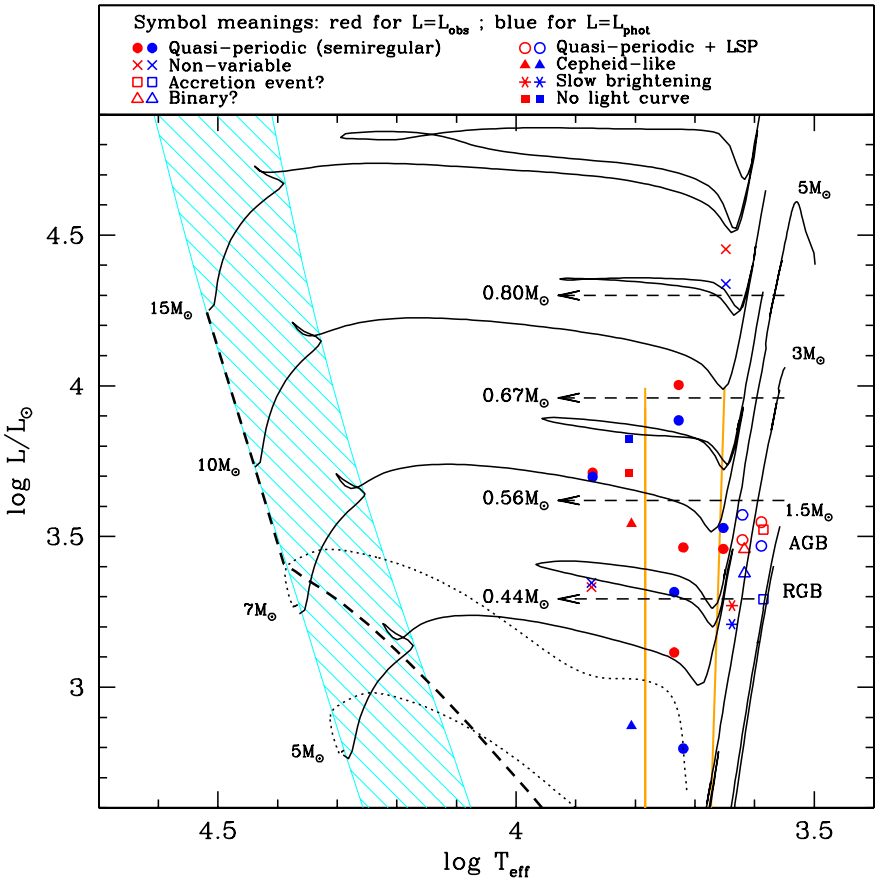

Figure 5. The HR diagram for the stars with TiO bands in emission. Each star is shown twice, using red symbols for $L_{\rm obs}$ and blue symbols for $L_{\rm phot}$. The symbol shapes depend on the variability type (see the legend at the top of the figure and Section 4 for details). PMS evolutionary tracks from Tognelli, Moroni & Degl'Innocenti (2011) are shown as the dotted lines, while post-main-sequence tracks from Bertelli et al. (2008) and Bertelli et al. (2009) are shown as the continuous lines. The initial stellar masses of the tracks are shown in the figure. Only the RGB and AGB phases of 1.5 and 3 $M_{\odot}$ stars are luminous enough to be seen in the figure. Schematic post-AGB and post-RGB evolutionary tracks are shown as the dashed lines with their masses marked (see text for details). The thick dashed line is the birth line for YSOs from Palla & Stahler (1999) with its extension above 7 $M_{\odot}$ as given by Bernasconi & Maeder (1996). The cyan hashed region shows the main-sequence area. The orange lines delineate the instability strip for RV Tauri stars in the LMC from Soszyński et al. (2008).

$T_{\rm eff}$ = 6000 K. For two stars, a status could not be assigned because the estimated log g was almost mid-way between the PMS and post-RGB/AGB values.

Although some of the objects in our sample have been assigned the PMS status on the basis of their gravities, there is a problem with the existence of optically-visible PMS stars in the part of the HR diagram where these objects are observed. PMS stars to the right of the 'birth line' shown in Fig. 5 should not be seen optically (Stahler 1985; Palla & Stahler 1990; Bernasconi & Maeder 1996; Palla & Stahler 1999) since the stars would have evolved to the birth line or beyond before the optically-thick accretion process has completed. A possible way around this would be to invoke an asymmetry in the accretion process that would allow the central star to be seen through a gap in the surrounding material (e.g. along the pole of the accretion disc). The birth line shown in Fig. 5 was computed for Galactic stars with a Galactic Population I abundance. The lower abundance in the SMC and LMC could make the circumstellar material more transparent so that PMS stars could be seen in an earlier phase of evolution. Indeed, Lamers, Beaulieu & de Wit (1999) and de Wit et al. (2005) invoked the lower metallicity of the LMC to explain the optical visibility of a group of PMS candidates in the LMC of O and B spectral type. We note that our PMS candidates are much cooler than those of Lamers et al. (1999) and de Wit et al. (2005) so that the effect of asymmetry or metallicity would need to be much more pronounced than for their stars. The evolutionary status, PMS or post-RGB/AGB, assigned here should be considered tentative.

At least one of the stars we have classified as a PMS star, J052023.97−695423.2, has in the past been classified consistently as a YSO, strongly suggesting a PMS status. It was observed as part of the SAGE-SPEC mid-IR spectral survey (Woods et al. 2011) and was classified as a YSO. It was found to have silicate dust emission, consistent with the oxygen-rich atmosphere that we have detected. J052023.97−695423.2 was also classified as a high-probability YSO in the study of Whitney et al. (2008) which used broad-band near- and mid-IR colours and luminosities to statistically separate various classes of objects.

Three of the objects show strong Li lines and several other stars show marginal detections (Fig. 6 and Table 1). Relatively strong Li lines are found in PMS stars only before the Li is destroyed by nuclear reactions in the stellar interior (e.g. Appenzeller & Mundt 1989). If this occurs when the star is convective to the surface, then the surface Li will be depleted. The PMS evolutionary tracks of Bernasconi & Maeder (1996) show that deuterium burning starts early in the evolution of stars with the luminosities observed here, at $T_{\rm eff} \sim$ 5000 K. The stars observed to have strong Li lines (J005355.00−731900.9, J051516.28−685539.7 and

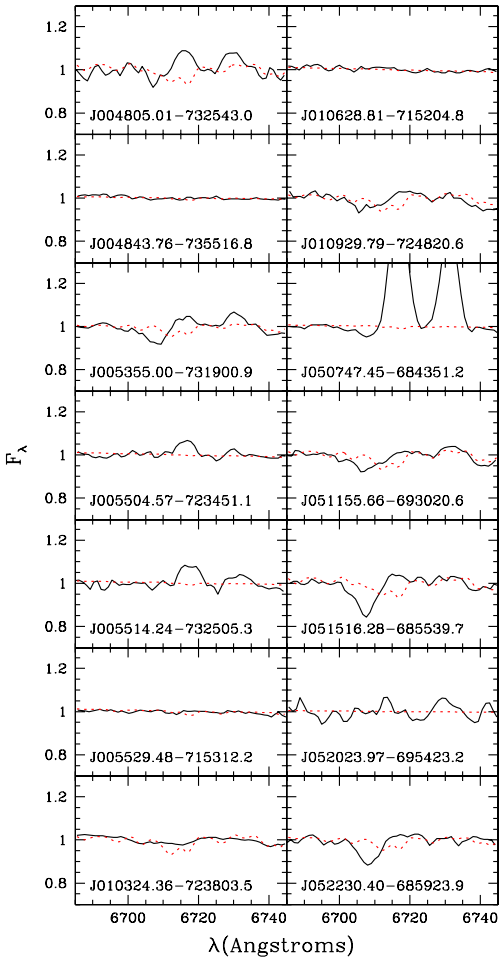

Figure 6. A small part of the spectrum of each of the stars covering the wavelength region of the Li 6708 Å and the [S II] 6717 and 6731 Å lines. The black lines are the observed spectra and the red dotted lines are the best-fitting model spectra.

J052230.40−685923.9) have $T_{\rm eff} < 5000$ K so the presence of the Li lines is consistent with the PMS status. In Table 1, one of these stars (J052230.40−685923.9) is considered a PMS star based on its log g value, while the other strong Li sources are a post-RGB star (J005355.00−731900.9) and a post-AGB star of low luminosity (J051516.28−685539.7, $L_{\rm phot} = 2943\,{\rm L}_{\odot}$). Strong Li lines are a feature of AGB evolution at higher masses and luminosities ($L \gtrsim 20000\,{\rm L}_{\odot}$) where hot-bottom burning occurs (Smith & Lambert 1990), but we do not expect strong Li lines in low-luminosity RGB or AGB stars. This suggests that J005355.00−731900.9 and J051516.28−685539.7 may also be PMS stars, contradicting their post-RGB/AGB status based on log g values.

4 VARIABILITY

Light curves from the MACHO (Alcock et al. 1992) and/or the OGLE II and OGLE III experiments (Udalski, Kubiak & Szymanski 1997; Szymanski 2005; Soszyñski et al. 2009; Soszyński et al. 2011) exist for 13 of the 14 stars in our sample, and they are shown in Fig. 7.

The stars show a range of types of variability. J005504.57−723451.1 and J010324.36−723803.5 are the only stars that show no detectable variability (the small annual variations that can be seen in the MACHO observations for J005504.57−723451.1 are an artefact of the data reduction). These stars are shown as crosses in Fig. 5.

Most other stars show variability that is a combination of a slow long-term brightening or fading and variability with periods from 30 d to more than 3000 d. The six stars J004805.01−732543.0, J005355.00−731900.9, J005514.24−732505.3, J010628.81−715204.8, J050747.45−684351.2 and J052023.97−695423.2 all show slow variations in magnitude over intervals longer than ∼1000 d, possibly due to slow changes in dust obscuration or variability in the rate of accretion.

J004805.01−732543.0 was fairly constant for the first 1500 d of observation after which it brightened by about 1 mag and exhibited an oscillation whose period decreased from ∼1150 d to ∼400 d over an interval of 4500 d. This oscillation is shown in Fig. 8 from JD−244 8800 = 1500 onwards after the long-term trend in magnitude was removed by fitting a fifth-order polynomial in time. The oscillation looks RV Tauri like (alternating deep and shallow minima), but it is unlikely that the interior structure of the star associated with this object could change enough on such a short time-scale that a period of pulsation could change by the observed amount. It is therefore likely that this phenomenon is associated with an accretion event in a surrounding disc, with disc viscosity causing the radius of the accreted material and orbital period to shrink rapidly. This star is shown as an open square in Fig. 5.

As well as the slow magnitude changes in J005355.00−731900.9, there is also an eclipse-like or RV Tauri-like variation with a period between deep minima of 193 d. The phased-up light curve in the interval 2000 < JD−244 8800 < 5000 is shown in Fig. 8 after the long-term trend was removed by fitting a fifth-order polynomial in time. Such a period seems too long for an RV Tauri star: Alcock et al. (1998) and Soszyński et al. (2008) find a maximum period of about 110 d for RV Tauri stars in the LMC and Soszyński et al. (2010) find a maximum period of about 100 d for RV Tauri stars in the SMC (in RV Tauri stars, the period is taken to be the time between the alternate deep minima). We suggest that J005355.00−731900.9 is a binary system with an orbital period of 193 d. This star is shown as an open triangle in Fig. 5.

J005514.24−732505.3 shows a smooth Cepheid-like light curve of increasing amplitude superimposed on the long-term variation. The period of 206 d is much longer than that of any Population II Cepheid in the MCs (Alcock et al. 1998; Soszyński et al. 2008, 2010), but the star lies close to the instability strip shown in Fig. 5 for these stars. The rapid increase in amplitude in this star suggests that it is rapidly evolving through the pulsational instability strip into a region where growth rates are larger. One problem with the interpretation of the 206 d cycle as pulsation is that when the amplitude reaches ∼1 mag, the light curve maintains a sinusoidal shape rather than changing to the saw-tooth shape typical of Cepheids with this amplitude. It is possible that the 206 d variation has some other explanation such as binarity. This star is shown as a filled triangle in Fig. 5.

The stars J004843.76−735516.8, J010628.81−715204.8, J010929.79−724820.6, J050747.45−684351.2, J051516.28−685539.7, J052023.97−695423.2 and J052230.40−685923.9 display quasi-periodic variability with periods of ∼30–160 d. Their periods are listed in Table 1 when they could be determined. Three of the stars are of spectral type K where semiregular variability frequently occurs in normal red giant stars but two have earlier F and G spectral types. Two of the K stars (J010929.79−724820.6 and J051516.28−685539.7) also exhibit the long secondary periods

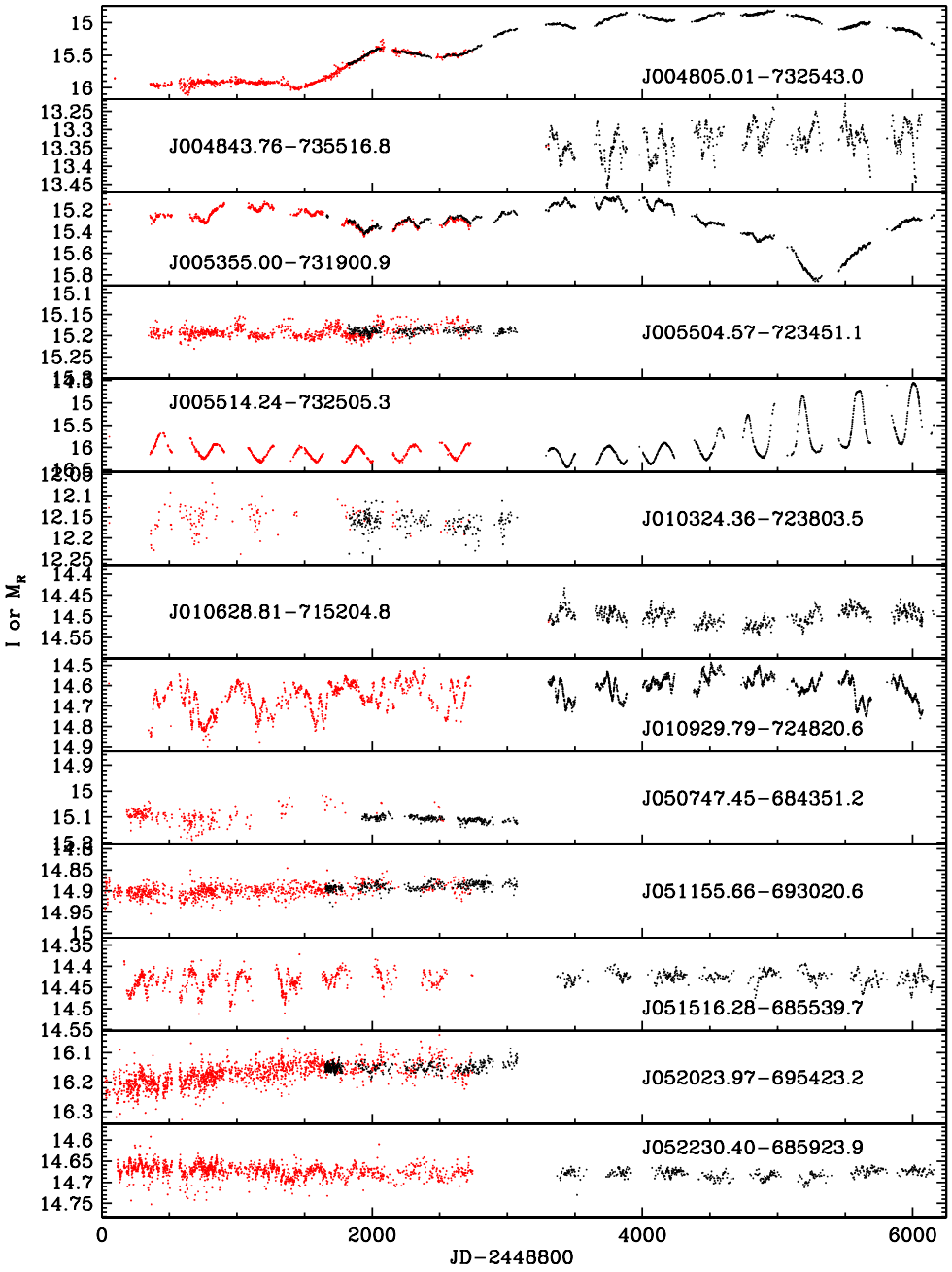

Figure 7. Light curves for 13 of the sources. The black curves for dates later than JD−244 8800 > 3250 are from OGLE III, the black curves with 1700 < JD − 244 8800 < 3250 are from OGLE II, while the red curves with 0 < JD − 244 8800 < 2800 are observed MACHO red magnitudes M_R normalized to the OGLE I magnitudes over the interval 2000 < JD − 244 8800 < 3250.

(LSPs) found in roughly one-third of variable red giants (Wood et al. 1999; Percy & Bakos 2003; Soszyński et al. 2007; Fraser, Hawley & Cook 2008). The quasi-periodic variables are shown as filled circles in Fig. 5, unless they have an LSP in which case they are shown as open circles.

The remaining star with a light curve, J051155.66−693020.6, has slowly brightening I and MACHO red (M_R) magnitudes with no evidence for other variability. It is shown as a star symbol in Fig. 5. The star with no light curve (J005529.48−715312.2) is shown as a filled square.

Overall, variability characteristics do not seem to help us distinguish between PMS stars and post-RGB or post-AGB stars. Of the six stars that show slow long-term variations in magnitude, three have been classified as post-RGB stars and three as PMS stars based on their estimated log g values. The star with Cepheid-like variability is listed as a PMS star based on log g, whereas Cepheid-like variability is known to occur in Population II Cepheids (although at shorter periods) which are post-AGB or post-RGB stars. Of the stars whose quasi-periodic variations look similar to those of red giant semiregular variables, three are classified as PMS stars and two as post-RGB/AGB stars (and two have no classification based on log g). It is perhaps not surprising that variability characteristics are not an unambiguous pointer to the evolutionary state. Both PMS stars and post-RGB/AGB stars are expected to be surrounded

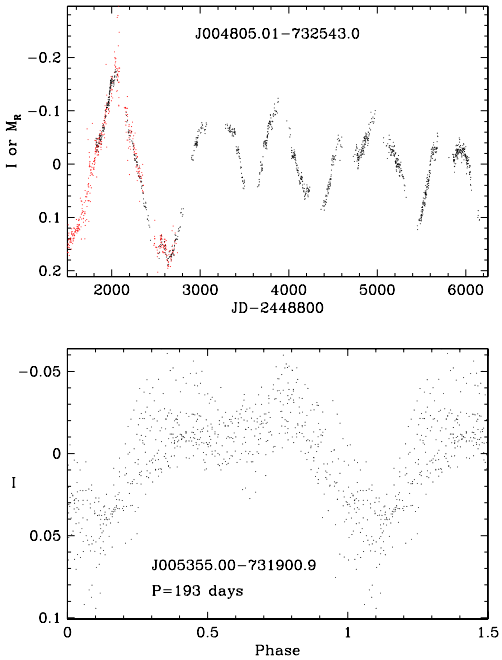

Figure 8. The light curves of J004805.01−732543.0 and J005355.00−731900.9 after long-term trends have been removed in the intervals 1500 < JD−244 8800 < 6250 and 2000 < JD−244 8800 < 5000, respectively. The light curve of J005355.00−731900.9 has been folded with a period of 193 d. Point colours are as in Fig. 7.

by large amounts of circumstellar dust that is clearing so that long-term slow changes in brightness would be expected in both cases. Similarly, both groups of stars originate on the Hayashi track and cross the instability strip so they might be expected to show the same type of pulsational variability, although the PMS stars should have shorter periods at a given luminosity because of their higher mass.

5 INDIVIDUAL OBJECT SUMMARY

Given the various results presented above, we provide here a synthesis of the properties of each object and comment on the possible evolutionary state. As a starting point, it should be remembered that all of these objects have both a strong mid-IR excess and TiO bands in emission so that they all have dense, warm and dusty circumstellar material in close proximity to the central star.

J004805.01−732543.0. The most remarkable feature of this star is the light curve which shows a 1 mag brightening starting at JD − 244 8800 = 1500 followed by a peak brightness around JD − 244 8800 = 5000 and a fading thereafter (Fig. 7). During this phase, there is an oscillation in the light curve with a period that decreases from 1150 to 400 d. Such rapid changes in brightness and period are most likely associated with the outer layers of the star or the circumstellar environment. An accretion event in a circumstellar disc is a plausible explanation. The star shows Hα emission and this is a possible direct indicator of the existence of a circumstellar disc. The estimated effective temperature ($T_{\rm eff} \sim 3849$ K) and luminosity (1960–3492 $L_\odot$) put the star close to the low-mass giant branch. The gravity estimate ($\log g = 0.0$) suggests that the star is a post-RGB star.

J004843.76−735516.8. This star has very strong TiO band emission, no Hα emission, a relatively warm temperature of 5300–5500 K and a relatively high luminosity of 7677–10067 $L_\odot$. The gravity estimate ($\log g = 0.8$) lies between that expected for a post-AGB or a PMS star of the given $T_{\rm eff}$ and L. The star shows a quasi-periodic variability and could be classified as an SRd variable because of its G0 spectral type. There is no strong evidence favouring either the post-AGB or the PMS status.

J005355.00−731900.9. This is a cool star ($T_{\rm eff} \sim$ 4140–4250 K) whose gravity estimate ($\log g \sim 0.0$) puts it in the post-RGB/AGB class. The cool $T_{\rm eff}$, well to the right of the birth line, also favours a post-RGB/AGB status. The two luminosity estimates put it near the RGB tip or just above on the AGB. It has Li 6708 Å absorption suggesting it could be a PMS star. The pointers to the PMS or post-RGB/AGB status for this star are in conflict. The light curve has prominent long-term variations of amplitude ∼0.6 mag as well as a periodic component. We suggest that this star is a binary with a period of 193 d.

J005504.57−723451.1. This is the hottest star in our sample with ($T_{\rm eff} \sim$ 7480–8900 K), yet it still has prominent TiO emission. It has broad Hα emission [intrinsic full width at half-maximum (FWHM) $\sim$ 235 km s^{-1}], possibly suggesting the presence of a circumstellar disc. The star does not seem to vary. The estimated gravity is high ($\log g \sim 3$), suggesting the star is a PMS star. The luminosity of the star ($L \sim$ 2148–2220 $L_\odot$) means that the stellar mass in this case is ∼8 $M_\odot$.

J005514.24−732505.3. This object has two remarkable features. First, its SED shows a dominant mid-IR peak and a smaller peak in the optical, indicating a central star that is highly obscured and seen mainly in scattered light. Secondly, the star shows a smooth, periodic, Cepheid-like variation with a period of 206 d whose amplitude increases from about 0.5 to 1.3 mag over an interval of about 1500 d. The origin of the 206 d variation is probably pulsation, although some other cause such as binarity cannot be excluded. The luminosity of the central star is highly uncertain and the estimates are 743 and 3486 $L_\odot$. The star is relatively warm ($T_{\rm eff} \sim$ 6404–6640 K) and the gravity estimate of $\log g = 2.5$ suggests that it is a PMS star. The luminosity estimates yield a stellar mass in the range 6–9 $M_\odot$ in this case.

J005529.48−715312.2. This is a relatively warm star ($T_{\rm eff} \sim$ 6457–7690 K) with a relatively high luminosity ($L \sim$ 5141–6668 $L_\odot$). With the estimated $\log g = 2.1$, it appears to be a PMS star. The luminosity estimate is consistent with a stellar mass of ∼12 $M_\odot$ in this case. There is no light curve for this star.

J010324.36−723803.5. This is the most luminous of our objects with $L \sim$ 21 757–28 384 $L_\odot$. It also has a relatively warm effective temperature $T_{\rm eff} \sim$ 4447–5500 K. The gravity $\log g = 0.0$ suggests it is a post-AGB star. This conclusion is supported by the unusually strong line observed at 6500 Å which is caused by the pair of lines 6496.89 Å of Ba II and 6498.76 Å of Ba I. The element Ba is produced by the s-process in AGB stars and it is brought to the stellar surface by the third dredge-up at helium shell flashes. The light curve of this star shows no variability.

J010628.81−715204.8. This is the second hottest star in the sample ($T_{\rm eff} \sim$ 7443–8450 K) and it is relatively luminous ($L \sim$ 4988–5031 $L_\odot$). The Hα line is in emission and it has a P Cygni profile suggesting a wind outflow with a velocity ∼430 km s^{-1}. The Ca triplet lines are also in emission. The estimated gravity ($\log g = 2.5$) indicates that the star is a PMS star. In this case, the stellar mass is ∼11 $M_\odot$. The light curve shows small-amplitude variations with a period of 33.5 d as well as long-term variations in mean magnitude.

J010929.79−724820.6. This is a cool star ($T_{\rm eff} \sim$ 4000–4173 K) with a moderate luminosity ($L \sim$ 3079–3732 $L_\odot$) that puts it above the RGB tip. The TiO emission bands are particularly strong but the mid-IR excess is relatively weak. The estimated gravity ($\log g = 0.7$)

lies between that of a post-AGB star and a PMS star. The light curve is typical of the semi-regular red giants that show a primary oscillation (in this case 70–100 d) as well as an LSP (in this case 444 d). We are unable to decide between the post-AGB or PMS status for this star.

J050747.45−684351.2. This a low-luminosity object ($L \sim 1304$–$2068\,L_\odot$) with a warm temperature ($T_{\rm eff} \sim 4850$–5430 K). The gravity estimate ($\log g = 0.5$) indicates that it is a post-RGB star. This object is listed as a YSO candidate by Whitney et al. (2008), although not of high probability. The light curve shows a slow variation in the mean magnitude and a very small amplitude oscillation with a period of around 50 d. The Hα line is in emission with a P Cygni profile consistent with a wind outflow of $\sim$350 km s^{-1}.

J051155.66−693020.6. This is another low-luminosity object ($L \sim 1618$–$1865\,L_\odot$) with a moderately warm temperature ($T_{\rm eff} \sim 4096$–4850 K) and a gravity estimate ($\log g = 0.0$), indicating that it is a post-RGB star. The TiO band emission is relatively weak. This object is listed as a YSO candidate by Whitney et al. (2008), although not of high probability. The light curve shows a very slow brightening.

J051516.28−685539.7. This is a cool star ($T_{\rm eff} \sim 3878$ K) of moderate luminosity ($L \sim 2943$–$3529\,L_\odot$). The gravity estimate ($\log g = 0.0$) suggests that it is a post-AGB star. The TiO band emission is relatively weak. The star shows variability typical of a red giant semiregular variable with a primary period of 124 d and an LSP of 380 d. The strong Li 6708 Å line suggests that the star may be a PMS star. This object is listed as a YSO candidate by Whitney et al. (2008), although not of high probability. The post-AGB or PMS status of this object is very uncertain.

J052023.97−695423.2. The luminosity of this object is dominated by the mid-IR flux, which is still rising at the longest detected wavelength of 24 μm. The star appears to be quite warm ($T_{\rm eff} \sim 5244$ K) and well away from the giant branch. There is a strong and broad Hα emission line of intrinsic FWHM ~ 424 km s^{-1} and wings extending out to 900 km s^{-1}. Like J005514.24−732505.3, the two luminosity estimates (626 and 2907 $L_\odot$) are quite different because of the dominance of the mid-IR flux. The gravity estimate ($\log g = 2.0$) suggests the star is a PMS star. The object has previously been classified as a high-probability YSO by Whitney et al. (2008). As a PMS star, the luminosity estimates suggest a stellar mass in the range $\sim$7–10 $M_\odot$. The light curve shows a slowly brightening magnitude as well as a short period (tens of days) oscillation of low amplitude.

J052230.40−685923.9. This is a cool star ($T_{\rm eff} \sim 4493$ K) of moderate luminosity (2876–$3375\,L_\odot$) whose gravity estimate ($\log g = 1.6$) suggests that it is a PMS star. The strong Li 6708 Å line supports the PMS status. As a PMS star, the luminosity estimate suggests a stellar mass of $\sim$9 $M_\odot$, although this is very uncertain since such a cool star is on the steeply sloped Hayashi track. It has strong TiO band emission. The light curve shows a small-amplitude variation with a period of 46 d.

6 SUMMARY AND CONCLUSIONS

We have discovered 14 stars in the MCs that have both a mid-IR flux excess and TiO bands in emission in the optical part of the spectrum. These features suggest that the stars have dense, hot dust and gas in their immediate circumstellar environments. Effective temperatures have been estimated for the objects from the optical spectra, reddening estimates have been made and the luminosities of the central stars derived. The position of the stars in the HR diagram suggests that they are either post-AGB or post-RGB stars of mass $\sim$ 0.4–0.8 $M_\odot$ or PMS star YSOs with masses of $\sim$7–19 $M_\odot$. We have tentatively assigned the stars to one of these two categories based on gravity estimates for the central stars, although for two of the stars this was not possible. We estimate that there are roughly equal numbers of PMS stars and post-RGB/AGB stars in our sample of TiO emitters. Those stars that are PMS stars are in an evolutionary stage well before the birth line where Galactic PMS stars are first assumed to become optically visible. Asymmetries in circumstellar material or the lower metallicity of the SMC and LMC may allow PMS stars to be visible in early evolutionary stages before the Galactic birth line. Those that are post-RGB stars must have formed as a result of binary interaction on the RGB. Similarly, those that are post-AGB stars must have formed as a result of binary interaction on the AGB since single AGB stars in the MCs become carbon stars before they leave the AGB to become post-AGB stars, yet these stars are all oxygen-rich. A circumbinary disc is expected in binary systems that have recently interacted and such discs can explain the presence of dense warm dusty circumstellar material in post-RGB and post-AGB stars.

The light curves of a majority of the stars show gradual brightening or fading, consistent with the presence of a changing circumstellar environment. One of the stars, J004805.01−732543.0, shows what looks like an accretion event that causes variability with a rapidly decreasing period. The star J005355.00−731900.9 has a light curve suggesting that it is currently an eclipsing binary system, while the star J005514.24−732505.3 has Cepheid-like pulsations that are increasing rapidly in amplitude, suggesting a rapid rate of evolution. Seven of the stars show quasi-periodic variability with periods of $\sim$30–160 d.

ACKNOWLEDGEMENTS

We are grateful to the referee, Greg Sloan, whose careful comments led to a number of improvements to the paper. This paper utilizes public domain data obtained by the MACHO Project, jointly funded by the US Department of Energy through the University of California, Lawrence Livermore National Laboratory under contract No. W-7405-Eng-48, by the National Science Foundation through the Center for Particle Astrophysics of the University of California under cooperative agreement AST-8809616, and by the Mount Stromlo and Siding Spring Observatory, part of the Australian National University. We also acknowledge the use of light-curve data obtained by the OGLE project as cited in the text.

REFERENCES

Alcock C. et al., 1992, in Fillipenko A. V., ed., ASP Conf. Ser. Vol. 34, Robotic telescopes in the 1990s. Astron. Soc. Pac., San Francisco, p. 193
Alcock C. et al., 1998, AJ, 115, 1921
Appenzeller I., Mundt R., 1989, A&AR, 1, 291
Bernasconi P. A., Maeder A., 1996, A&A, 307, 829
Bertelli G., Girardi L., Marigo P., Nasi E., 2008, A&A, 484, 815
Bertelli G., Nasi E., Girardi L., Marigo P., 2009, A&A, 508, 355
Blum R. D. et al., 2006, AJ, 132, 2034
Cardelli J. A., Clayton G. C., Mathis J. S., 1989, ApJ, 345, 245
Castelli F., Kurucz R. L., 2004, preprint (astro-ph/0405087)
Cohen M., Van Winckel H., Bond H. E., Gull T. R., 2004, AJ, 127, 2362
Covey K. R. et al., 2011, AJ, 141, 40
de Ruyter S., van Winckel H., Maas T., Lloyd Evans T., Waters L. B. F. M., Dejonghe H., 2006, A&A, 448, 641
de Wit W. J., Beaulieu J. P., Lamers H. J. G. L. M., Coutures C., Meeus G., 2005, A&A, 432, 619

Fraser O. J., Hawley S. L., Cook K. H., 2008, AJ, 136, 1242
Gordon K. D. et al., 2011, AJ, 142, 102
Gray R. O., Corbally C. J., 2009, Stellar Spectral Classification. Princeton Univ. Press, Princeton
Groenewegen M. A. T. et al., 2007, MNRAS, 376, 313
Han Z., Podsiadlowski P., Eggleton P. P., 1995, MNRAS, 272, 800
Hillenbrand L. A., Knapp G. R., Padgett D. L., Rebull L. M., McGehee P. M., 2012, AJ, 143, 37
Kamath D., Wood P. R., Van Winckel H., 2013, MNRAS, submitted
Keller S. C., Wood P. R., 2006, ApJ, 642, 834
Lamers H. J. G. L. M., Beaulieu J. P., de Wit W. J., 1999, A&A, 341, 827
Meixner M. et al., 2006, AJ, 132, 2268
Men'shchikov A. B., Schertl D., Tuthill P. G., Weigelt G., Yungelson L. R., 2002, A&A, 393, 867
Munari U., Sordo R., Castelli F., Zwitter T., 2005, A&A, 442, 1127
Neilson H. R., Ngeow C.-C., Kanbur S. M., Lester J. B., 2010, ApJ, 716, 1136
Palla F., Stahler S. W., 1990, ApJ, 360, L47
Palla F., Stahler S. W., 1999, ApJ, 525, 772
Percy J. R., Bakos A. G., 2003, in Gray R. O., Corbally C. J., Philip A. G. D., eds, The Garrison Festschrift. L. Davis Press, Schenectady, p. 49
Pickles A. J., 1998, PASP, 110, 863
Porter J. M., Rivinius T., 2003, PASP, 115, 1153
Smith V. V., Lambert D. L., 1990, ApJ, 361, L69
Smith G. A. et al., 2004, in Moorwood A. F. M., Masanori I., eds, Proc. SPIE Vol. 5492, Ground-based Instrumentation for Astronomy. SPIE, Bellingham, p. 410
Soszyński I. et al., 2007, Acta Astron., 57, 201
Soszyński I. et al., 2008, Acta Astron., 58, 293
Soszyński I. et al., 2009, Acta Astron., 59, 239
Soszyński I. et al., 2010, Acta Astron., 60, 91
Soszyński I. et al., 2011, Acta Astron., 61, 217
Stahler S. W., 1985, ApJ, 293, 207
Szymanski M. K., 2005, Acta Astron., 55, 43
Tognelli P. G., Moroni P. G., Degl'Innocenti S., 2011, A&A, 533, A109
Udalski A., Kubiak M., Szymanski M., 1997, Acta Astron., 47, 319
van de Steene G. C., Wood P. R., van Hoof P. A. M., 2000, in Kastner J. H., Soker N., Rappaport S., eds, ASP Conf. Ser. Vol. 199, Asymmetrical Planetary Nebulae II: From Origins to Microstructures. Astron. Soc. Pac., San Francisco, p. 191
Van Winckel H., 2004, Mem. Soc. Astron. Ital., 75, 766
Vassiliadis E., Wood P. R., 1993, ApJ, 413, 641
Whitney B. A. et al., 2008, AJ, 136, 18
Wood P. R. et al., 1999, in Le Bertre T., Lebre A., Waelkens C., eds, Proc. IAU Symp. 191, Asymptotic Giant Branch Stars. Astron. Soc. Pac., San Francisco, p. 151
Woods P. M. et al., 2011, MNRAS, 411, 1597
Wright E. L. et al., 2010, AJ, 140, 1868
Zaritsky D., Harris J., Thompson I. B., Grebel E. K., Massey P., 2002, AJ, 123, 855
Zaritsky D., Harris J., Thompson I. B., Grebel E. K., 2004, AJ, 128, 1606
Zickgraf F.-J., Wolf B., Stahl O., Humphreys R. M., 1989, A&A, 220, 206

This paper has been typeset from a TEX/LATEX file prepared by the author.